ELSEVIER

Contents lists available at ScienceDirect

Journal of Neuroscience Methods

journal homepage: www.elsevier.com/locate/jneumeth





Prediction of gender from longitudinal MRI data via deep learning on adolescent data reveals unique patterns associated with brain structure and change over a two-year period

Yuda Bi^{*}, Anees Abrol, Zening Fu, Jiayu Chen, Jingyu Liu, Vince Calhoun

Tri-Institutional Center for Translational Research in Neuroimaging and Data Science (TReNDS), Georgia Tech, Emory, Atlanta, Georgia State 30303, Georgia

ARTICLE INFO

Keywords: Structural MRI Deep Learning Brain Visualization Gender Classification

ABSTRACT

Deep learning algorithms for predicting neuroimaging data have shown considerable promise in various applications. Prior work has demonstrated that deep learning models that take advantage of the data's 3D structure can outperform standard machine learning on several learning tasks. However, most prior research in this area has focused on neuroimaging data from adults. Within the Adolescent Brain and Cognitive Development (ABCD) dataset, a large longitudinal development study, we examine structural MRI data to predict gender and identify gender-related changes in brain structure. Results demonstrate that gender prediction accuracy is exceptionally high (>97%) with training epochs > 200 and that this accuracy increases with age. Brain regions identified as the most discriminative in the task under study include predominantly frontal areas and the temporal lobe. When evaluating gender predictive changes specific to a two-year increase in age, a broader set of visual, cingulate, and insular regions are revealed. Our findings show a robust gender-related structural brain change pattern, even over a small age range. This suggests that it might be possible to study how the brain changes during adolescence by looking at how these changes are related to different behavioral and environmental factors.

1. Introduction

Deep learning (DL) has steadily risen to become the mainstream technique for analyzing big data for complex problems over the last decade, owing to its outstanding performance on a wide range of challenging tasks and the rapid growth in computing resources available (Hinton, 2018; Krizhevsky et al., 2017; Shen et al., 2017). Also demonstrated is the ability of DL models to improve the prediction and analysis of specific biomedical imaging data modalities, including computed tomography (CT), magnetic resonance imaging (MRI), magnetoencephalography (MEG), and positron emission tomography (PET) (Miller et al.), to name a few examples (Yan et al., 2022). As medical imaging data is very high-dimensional and complex, automated approaches are needed to identify the relevant information for a given task. Therefore, it is critical to continue developing and evaluating the efficacy of DL models. Initial work suggests that deep learning on neuroimaging data shows promise for accelerating the identification of diagnostic subtypes in mental disorders (Yan et al., 2021), with the potential for expanding into clinically relevant tasks such as prediction of medication class response (Osuch et al., 2018). U-Net (Ronneberger

et al., 2015), one of the most successful deep learning architectures for medical image segmentation, is an important starting point for utilizing deep learning models in medical image analysis. Other applications include the ability to classify different chest illnesses using X-ray imaging datasets that have been compiled from thousands of patient records and physician diagnoses(Wang et al., 2017).

The human brain is a highly complex organ that is not fully understood through research in medical imaging data. It is critical for researchers to develop a more effective method of identifying brain disorders (Liu et al., 2020). Deep learning has performed well for image classification and segmentation tasks in brain imaging as a sophisticated and highly flexible artificial intelligence system (Shahamat and Saniee Abadeh, 2020; Zhang et al., 2020a). When using T_1 -weighted MRI, also known as structural MRI, one can visualize specific brain areas and structures, which can help diagnose a problem or potentially predict how a person will respond or behave in the future. For image classification problems, especially in datasets of natural image examples, various common machine learning methods, such as support vector machine (SVM), have historically been used. However, the SVM's performance for medical imaging subjects suffers under some

E-mail address: ybi3@student.gsu.edu (Y. Bi).

 $^{^{\}ast}$ Corresponding author.

circumstances, especially when working with high-resolution T1-weighted MRI images (Chato and Latifi, 2017). Deep learning models have shown great promise for neuroimaging data (Plis et al., 2014; Varatharajah et al., 2018; Yan et al., 2022). It has recently been demonstrated that deep learning models outperform traditional machine learning approaches in a wide range of classification and regression tasks (Abrol et al., 2021). For example, a fully convolutional network (FCN) is a tool that is particularly well-suited for image segmentation tasks, such as distinguishing brain tumors from normal brain tissues (Chen et al., 2021; Justin et al., 2017). Various prediction and regression tasks, such as brain age and gender prediction (Brennan et al., 2021), have been efficiently and effectively performed by deep learning approaches, such as 3-D convolutional neural networks (CNNs). Deep learning models like auto-encoders, deep belief networks (DBN), and generative adversarial networks (GAN) have also been very important to the development of AI and medical image analysis (Reddy et al., 2020; Sorin et al., 2020).

In this work, we explore a large longitudinal development study (the Adolescent Brain and Cognitive Development (ABCD) dataset) to examine structural MRI data to predict gender and identify genderrelated changes in brain structure. The ABCD study is a prospective longitudinal neuroimaging study that recruits children with 9-10 years old and follows them for ten years (Casey et al., 2018; Karcher and Barch, 2021). There are 21 research sites across the country participating in the study, which includes a diverse sample of nearly 12,000 subjects. For this study, we used T₁-weighted MRI data from the ABCD dataset, which contains (N > 11 K) subjects at baseline and 3 K subjects at a year two follow-up, to evaluate gender prediction and to visualize the predictive brain regions in the context of multiple learning tasks on the dataset. We use 3D CNN models to allow the model to leverage the 3D information in brain structural MRI data. We are particularly interested in determining whether or not we can accurately and reliably predict gender from neuroimaging data collected from developing adolescents. In our research, we used 3D AlexNet as the CNN backbone to predict gender, and we found that it performed exceptionally well in terms of accuracy and robustness when applied to the ABCD baseline dataset. Meanwhile, we investigated prediction on data collected two years later and discovered that the accuracy of gender prediction was slightly, but significantly, higher than baseline in these subjects. Moreover thirdly, we performed a longitudinal prediction on gray matter differences over two years. We present the findings in the form of ROI-based brain saliency maps averaged within the automated anatomical labeling (AAL) atlas(Gupta et al., 2019), which demonstrates brain regions that are highly relevant in gender prediction and how these regions change longitudinally between the baseline and two-year follow scans.

Below is a list of the contributions we include in this paper:

- We developed an effective and light-weighted 3-D deep learning model for analyzing gender prediction problems in adolescent individuals using structural MRI data, and the model's performance was outstanding and robust in the real world.
- 2. We verified gender prediction cross-sectionally and longitudinally, and new findings have occurred.
- Brain regions most salient to the baseline and two-year prediction and the prediction from the differences are visualized. We highlight differences in brain structure between males and females and longitudinal changes between baseline and the two-year follow-up.

Our initial questions for this work were three-fold: 1) could deep learning of gray matter data with 3D CNNs provide higher accuracy for predicting M vs F in adolescent data than previous studies? 2) would the single image prediction (not difference) increase between baseline and year two?, and 3) how predictive are the changes between baseline and year 2? In addition, a key component for all three of these questions was also to visualize the relevant brain regions.

The remaining text is organized as follows: Section II introduces the underlying methodologies that correspond to CNN architectures and pipelines, methods used for ROI-based brain visualization; Section III displays experimental results, including gender prediction performance matrices and longitudinal results; saliency maps that show different weights in each ROI; and Section IV concludes the experimental meanings, future research directions, and some limitations of this paper.

2. Methods

Our previous work on adults from the UK Biobank demonstrated that DL models could extract powerful brain representations from 3D brain data, significantly outperforming traditional machine learning approaches (Abrol et al., 2021). This project uses the same pipeline with the 3D CNN model as the previous study to predict gender from structural MRI data in the ABCD dataset. We perform the gender classification task using two time points from this longitudinal study: the baseline and the two-year follow-up. In order to determine exciting brain regions relevant to gender prediction and longitudinal changes, we built saliency maps based on our DL model and selected ROIs of the brain. Fig. 1 provides an overview of the primary pipeline used in our project.

We work with three datasets: $D_1(N=11700)$ for the baseline cohort (ages 9–10 years old), $D_2(N=2928$ of 11700) for the follow-up cohort (ages 11–12 years old), and $D_3(N=2928$ of 11700) for the difference cohort (within-subject difference between baseline and two-year follow-up voxel-wisely). More precisely, we created a variety of datasets to be used for training, validation, and testing. We divided the datasets D_1 into a training set D_1^{tr} of subjects ($N^{tr}=9220$), a validation set D_1^{va} of subjects ($N^{va}=972$), and a testing set D_1^{te} of subjects ($N^{te}=972$). Because we did not use D_2 dataset for model training, it contains only a testing dataset D_2^{te} with ($N^{te}=2928$) subjects. For D_3 , It consists of a training set D_3^{tr} ($N^{tr}=2048$) and validation set D_3^{va} ($N^{va}=434$) subjects, as well as testing set D_3^{te} ($N^{te}=434$) subjects.

2.1. Data pre-processing

This work analyzes structural MRI data from the ABCD study at baseline and two years later. ABCD is one of the largest ongoing studies of adolescents, following over 11,000 youth recruited at the age of 9-10 through late adolescence to increase our understanding of the emotional, genetic, neurological, and behavioral factors associated with an increased risk of physical and mental health problems in adolescents: http://abcdstudy.org. The baseline (D1) and two-year follow-up (D2) datasets were segmented using the unified approach in the statistical parametric mapping (SPM) software. The difference dataset (D₃) was generated by subtraction between two-year and baseline in each subject for every voxel. We use SPM12 to jointly segment and normalize the sMRI data tissue probability maps for gray matter, white matter, and cerebral spinal fluid (CSF). The Montreal Neuroimaging Institute (MNI) space gray matter images used in this study had a dimensionality of $(121 \times 145 \times 121)$ voxels after the pre-processing, with a voxel size of $1.5 \times 1.5 \times 1.5$ mm². Tables 1 and 2.

2.2. CNN architecture

Our deep learning model is based on an updated three-dimensional AlexNet architecture (Krizhevsky et al., 2017) with a three-dimensional input size of ($121 \times 145 \times 121$). We created five blocks of 3-D convolutional layers with batch normalization. Each convolutional layer has a channel width of 64, 128, 192, 192, and 128. Following each batch normalization layer, the ReLU function was applied, followed by pooling layers. Finally, we created two fully connected layers with sizes of 256 and 64. After the first fully connected layer, we set the drop-out rate to 0.5. After the second fully connected layer, the number of output nodes was set to the number of classes

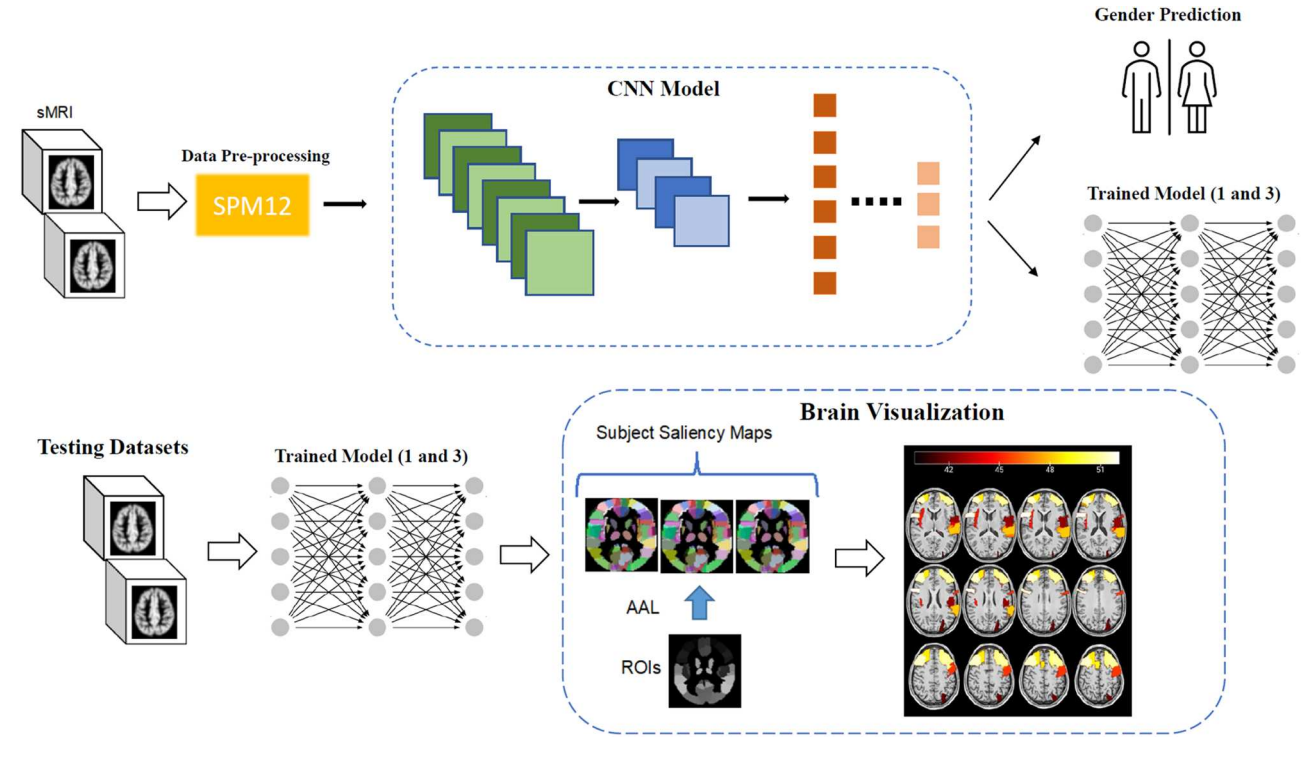


Fig. 1. General pipeline for gender prediction and estimating brain region saliency maps. The sMRI data were preprocessed using SPM12. The deep learning model was trained and tested using the preprocessed sMRI data, and brain saliency maps were generated using the AAL atlas.

Table 13-D AlexNet architecture details.

Layer	Feature Map	kernel Size	Stride	Activation
Convolution	64	(5, 5, 5)	(2, 2, 2)	Batchnorn+ReLU
MaxPooling		(3, 3, 3)	(3, 3, 3)	
Convolution	128	(3, 3, 3)	(1, 1, 1)	Batchnorn+ReLU
MaxPooling		(3, 3, 3)	(1, 1, 1)	
Convolution	192	(3, 3, 3)	(1, 1, 1)	Batchnorn+ReLU
Convolution	192	(3, 3, 3)	(1, 1, 1)	Batchnorn+ReLU
Convolution	128	(3, 3, 3)	(1, 1, 1)	Batchnorn+ReLU
MaxPooling		(3, 3, 3)	(1, 1, 1)	
Fully-	256		Drop-out rate	ReLU
Connected			0.5	
Fully-	64			ReLU
Connected				
Output	2			

(n = 2) required for the gender classification task. All experiments were conducted using the PyTorch machine learning framework on the NVI-DIA CUDA platform on NVIDIA Tesla V100 32 GB GPUs. Fig. 2.

2.3. Model training

For the gender prediction tasks, we designed three main experiments based on pre-processed datasets in ABCD. Firstly, we use D_1^{tr} as a training set $(N_{tr}=9220)$ to train 3-D AlexNet for first model M_1 (batch size = 32, learning rate = 1e-3, training algorithm = Adam, number of epochs = 200) and then use testing set in D_1^{te} to obtain results on baseline gender prediction. To obtain a robust performance measure, we employed a repeated (n=5), stratified k-fold (k=5) cross-validation strategy to create five different repetitions of training, validation, and testing datasets (same size as above), which were used for training five models. Then we record the average testing performance on the held-out test partitions. The Adam optimizer was employed with a 1e-3 initial learning rate that adapts as the epochs pass. An early stopping procedure

Table 2All gender prediction tasks and their corresponding brain regions.

Gender Predictions	Conditions	Active Brain Regions
Baseline Dataset Gender Prediction	General	Inferior, middle, and superior frontal and inferior temporal gyri
	M > F	Lingual gyrus (R), the supplementary motor area (R), Heschl's gyrus (R), and the cerebellum (L)
	F > M	Caudate nucleus (R), the putamen (L), the precuneus (L), and the middle temporal gyrus (L & R)
Two-year follow-up dataset gender	General	Inferior, middle, and superior frontal and inferior temporal gyri
prediction	M > F	Lingual gyrus (R), the supplementary motor area (R), Heschl's gyrus (R), and the cerebellum (L)
	F > M	Caudate nucleus (R), the putamen (L), the precuneus (L), and the middle temporal gyrus (L & R)
Related longitudinal	Baseline	Cuneus (L & R), insular cortex (R),
Comparison	> Two-year	cingulum posterior (L), and lingual gyrus (L) are some of the regions involved (L)
	Two-year	Caudate nucleus (R), the orbital section
	> Baseline	of the inferior frontal gyrus (R),
		cingulum anterior (L), and postcentral gyrus (L)
Difference dataset gender prediction	General	Inferior, middle, and superior frontal and inferior temporal gyri
	M > F	Precentral gyrus (L), superior temporal gyrus (L), middle temporal gyrus (L), superior frontal gyrus (L) and operculum (L)
	F > M	Hippocampus (R), superior temporal gyrus (R), middle temporal gyrus (R), ParaHippocampal (R) and Inferior temporal gyrus (R)

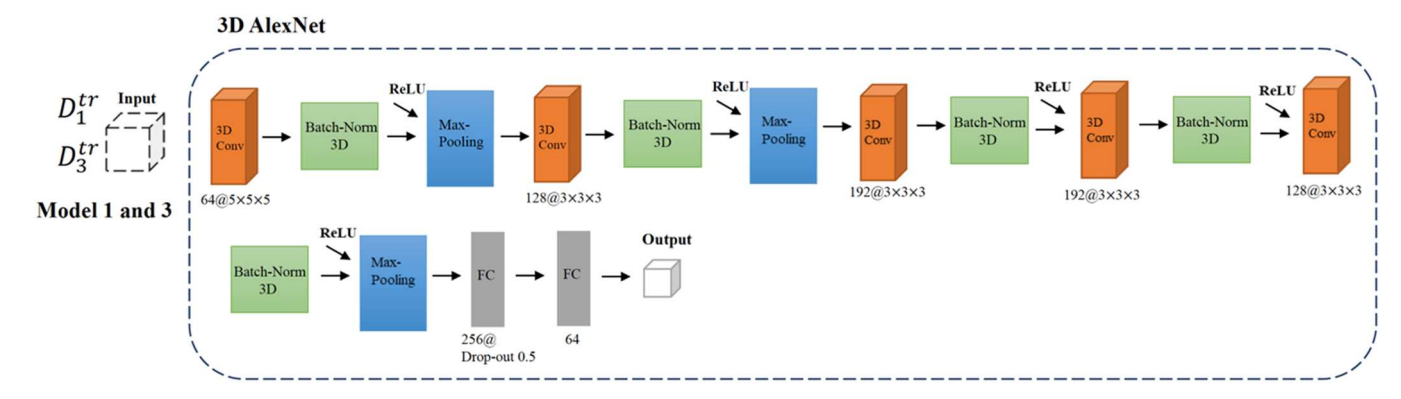


Fig. 2. Updated 3-D AlexNet CNN architecture. We trained model 1 and model 3 using same CNN architecture, which includes modified light-weighted 3-D AlexNet with batch normalizations and drop-out.

with a patience level of 20 epochs was used to avoid data overfitting. The accuracy (Acc), balanced accuracy (Bal-Acc), AUC score, F1 score, and Matthew's correlation coefficient (MCC) classification metrics were used to evaluate performance. Secondly, after training the CNN model with D_1 tr dataset, we evaluated the CNN model's generalization ability by testing on a two-year follow-up dataset D_2^{te} using Acc, Bal-Acc, AUC, F1, and MCC. Finally, to determine the features and gender prediction sensitivity related specifically to longitudinal changes over two years, we re-trained the second model M_3 using D_3^{tr} ($N^{tr} = 2048$) and tested it by D_3^{te} ($N^{te} = 434$). The validated model hyper-parameters include batch-size = 16, learning rate = 1e-3, training algorithm = Adam, number of epochs = 150. We reduced the batch size and number of epochs because the training set's size is significantly smaller than D_1 dataset.

2.4. Brain region visualization

We also perform DL model introspection to identify the most discriminative brain regions for the gender classification tasks. We compute voxel-wise saliency maps using the area occlusion approach (Abrol et al., 2021). This method used the AAL atlas as the occlusion template. The brain regions were occluded one at a time, and the class probabilities were then recomputed post-occlusion. The saliency was then estimated to be proportional to the reduction in the class probabilities after occlusion. Saliency maps were made by applying the CNN model to each test dataset and then using a region-wise t-test to fill each voxel with the right t-statistic.

3. Results

3.1. Gender prediction results

For gender prediction tasks, we test the performance of baseline gender prediction on the model M_1 using D_1^{te} by 5-fold cross-validation, resulting in an average balanced accuracy of 97.3%. The accuracy on D_2^{te} for longitudinal data (two-year) is 0.3–0.5% above the baseline performance. For the longitudinal changes, we test model M_3 accuracy by D_3^{te} using the same strategy as previous experiments and obtained an average balanced accuracy of 71%. To demonstrate the difference in accuracy between two-year and baseline, we used a paired t-test to compare the accuracy between the two. The results showed a t-value of 3.4 and a p-value of 0.0325, indicating a significant improvement in two-year gender prediction over the baseline. Fig. 3 shows the loss and accuracy curves during the training and validation process. Fig. 4 shows the detailed results (Acc, Bal-Acc, AUC, F1 score, and MCC) for our three main experiments.

Meanwhile, we used scatterplots and the t-distributed stochastic neighbor embedding (t-SNE) (Hinton and Roweis, 2002) algorithm to visualize the gender prediction results obtained by mapping the high-dimensional subjects to the two-dimensional space x and y. The tSNE algorithm is a nonlinear dimensionality reduction technique for visualizing large amounts of data by assigning each data point a location on a two- or three-dimensional map. The t-SNE algorithm can visualize clusters, which illustrate the classification model's performance. We use latent encodings estimated for the $D_1^{\rm te}$ ($N^{\rm te}=972$), $D_2^{\rm te}$ ($N^{\rm te}=2928$) and

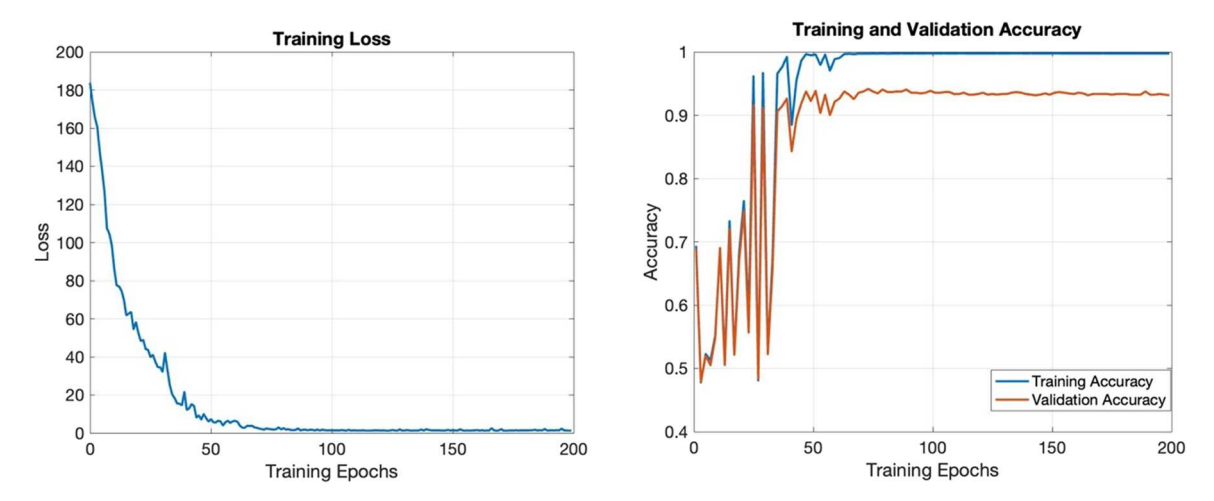


Fig. 3. Deep learning model training learning curves: training loss (left) and training and validation accuracy (right). The training and validation curves converge after 60 epochs with an average training time of 12.5 h with Nvidia Tesla V100 32 GB GPU.

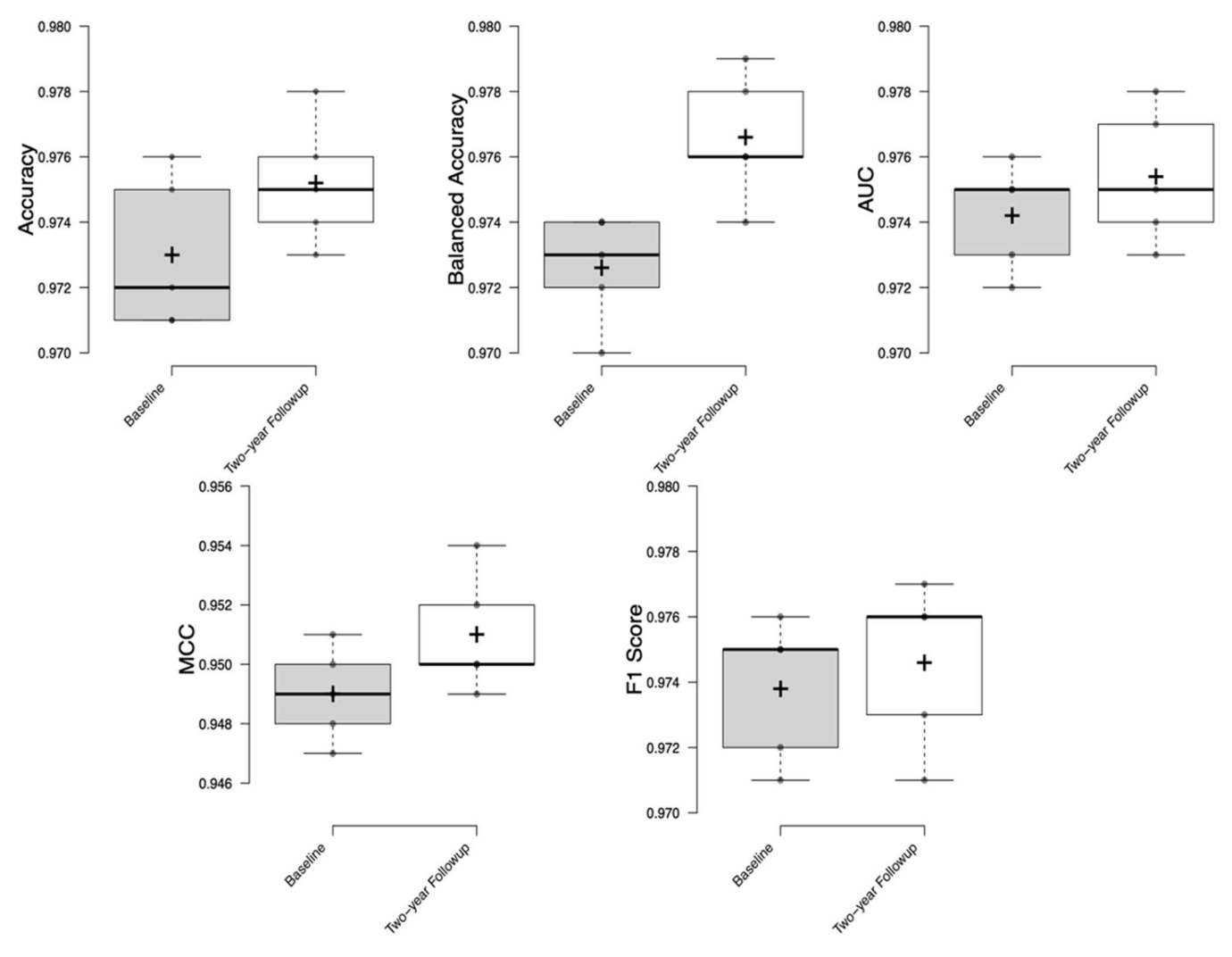


Fig. 4. Boxplots for baseline gender prediction accuracy, longitudinal gender prediction accuracy and the accuracy of gender prediction based on longitudinal changes show test data results based on a 5-fold cross-validation approach. P-value of 0.0325 in accuracies comparison indicates significant improvement in two-year follow-up data over baseline data.

 D_{1}^{tc} ($N^{te}=434$) datasets as inputs to three distinct t-SNE plots to evaluate prediction performance for baseline, two-year, and difference datasets. We pass D_{1}^{tc} ($N_{te}=972$) and D_{2}^{tc} ($N^{te}=972$) datasets through a trained model M_{1} and extract the 64-dimension features at the output of the first fully-connected layer as the input to the t-SNE algorithm. For D_{3}^{tc} ($N^{te}=434$), we pass it through model M_{3} and extract the same features as for D_{1}^{tc} and D_{2}^{tc} . Using t-SNE, we can reduce the 64-dimensional

features to two dimensions and visualize two male and female data points clusters. Fig. 5.

3.2. Brain saliency maps

Saliency maps can be used for brain region visualization to identify brain areas that are particularly predictive for gender classification. Using the test datasets, including $D_1^{te}(N^{te}=972)$, $D_2^{te}(N^{te}=2928)$ and

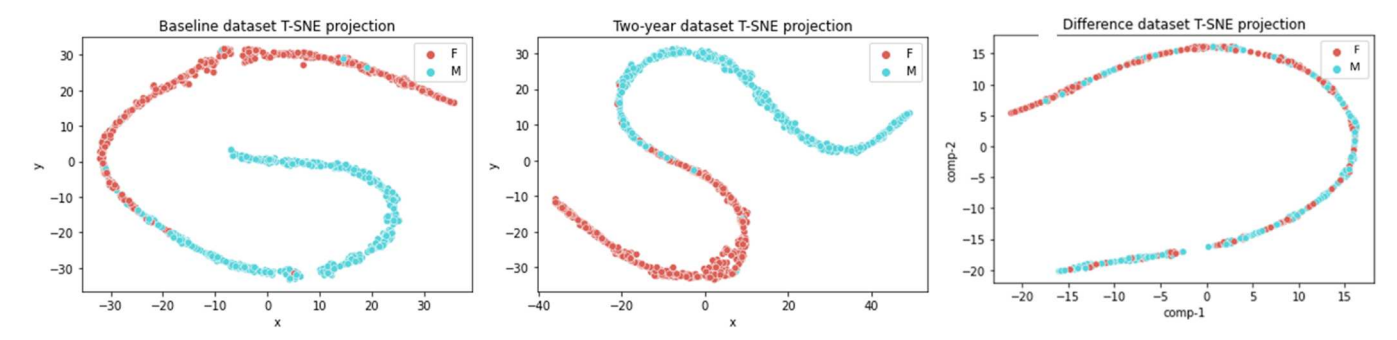


Fig. 5. Scatterplots for baseline, two-year and difference datasets based on t-SNE algorithm. Prediction from the full gray matter maps is highly accurate and increases significantly between baseline and two years. In addition, the two-year change in gray matter is also predictive well above chance. Focusing on the predictive regions relevant to longitudinal change can provide additional insights into the developing brain.

 $D_s^{tc}(N^{te}=434)$, we generated three groups S_1 , S_2 and S_3 of saliency maps for each subject (N = 972, 2928 and 434, respectively). The results include a one-sample t-test on the baseline and two-year testing datasets, which can be used to determine which brain regions are more significant and predictive in gender prediction tasks; a two-sample t-test on the baseline and two-year testing datasets that compare male and female subjects, which can be used to determine which brain regions are more significant in male subjects and which brain regions contribute more to female subject prediction. Meanwhile, to get more advanced and accurate results, we analyzed the brain areas that are most informative for the prediction from the longitudinal difference between two-year and baseline; we also computed one-sample t-tests to evaluate the most relevant brain areas for baseline and two-year. Figs. 6–9.

By analyzing saliency maps, baseline and two-year showed broadly similar patterns, including inferior, middle, and superior frontal and inferior temporal gyri. Meanwhile, the parts of the brain that predict a person's gender based on a difference dataset are also strongly linked to baseline and two-year datasets.

In addition, we performed a two-sample t-test on the test data to estimate t-values for each ROI. Parts of the brain where men are more predictive than women (M > F) are represented by positive t-values; areas of the brain where men are less predictive than women (M > F) are represented by negative t-values (M < F). When we looked at the baseline dataset, we discovered that M > F brain areas included the Lingual gyrus (R), the supplementary motor area (R), Heschel's gyrus (R), and the cerebellum (L); M < F brain areas included the caudate nucleus (R), the putamen (L), the precuneus (L), and the middle temporal gyrus (L & R). The brain regions studied for the two-year dataset are similar to those studied at baseline, although some have a different tvalue and a different order. We also discovered a t-test related to longitudinal data, and the positive t-values signify regions of the brain where baseline predictability is greater than two-year predictive validity. Cuneus (L & R), insular cortex (R), cingulum posterior (L), and lingual gyrus (L) are some of the regions involved (L). The findings, on the other hand, show that parts of the brain like the caudate nucleus (R),

the orbital section of the inferior frontal gyrus (R), the cingulum anterior (L), and the postcentral gyrus (L) are more accurate predictors in the two years than they were in the baseline period. Finally, we were able to predict gender using the differential data accurately. The cingulum posterior, angular gyrus, fusiform gyrus, and supramarginal gyrus were all identified in these findings. More crucially, we identified and mapped different locations associated with M>F and F>M, located in different brain hemispheres. Relevant regions in the right hemisphere are produced by the M>F condition, and relevant regions in the left hemisphere are produced by the M>F condition.

4. Discussion and conclusion

In conclusion, our work achieves a high degree of accuracy in brain gender analysis tasks, and our model was effectively evaluated using longitudinal data and a specific dataset to demonstrate its efficacy. Using structural MRI data from adolescents, our work delivers two unique contributions to the area of gender prediction. First, we begin by comparing recent findings from baseline data to longitudinal data from the ABCD dataset, which includes patients two years older than at baseline. We demonstrate that the testing accuracy of the two-year follow-up data is comparable to but substantially greater than that of the baseline data (0.3–0.5% higher than baseline). Brain saliency maps were also identified, which depict the essential brain areas for the prediction tasks, including gender and longitudinal comparison. Second, we employ an upgraded 3D-CNN model with great prediction accuracy performance.

Reviewing previous research, we discover that (Adeli et al., 2020; Adeli et al., 2020) conducted gender prediction trials on the ABCD dataset and reached an accuracy of 89.6%, which is lower than our results. In addition, they did not compare outcomes over times using follow-up data. Using a cutting-edge deep learning model, they compared deep learning to a conventional machine learning SVM model, reviewed the performance, and found morphological drivers in gender prediction using saliency mapping. Brennan et al. (2021) utilized

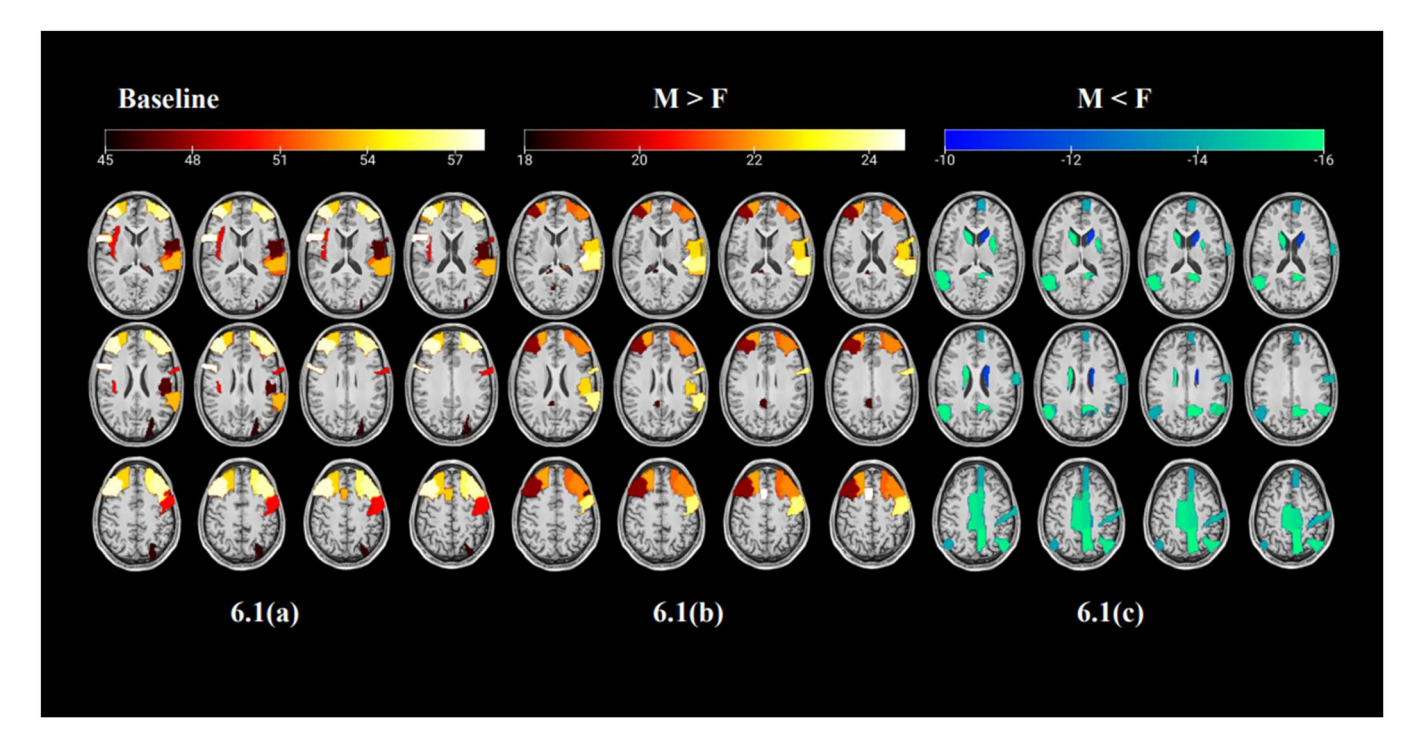


Fig. 6. Saliency maps generated from the baseline D_1 , two-year D_2 , and difference D_3 datasets. Figure 6.1(a) depicts one sample t-test on subject-level saliency maps from the D_1 testing datasets, which can reveal which brain regions are significantly more predictive than others for gender prediction; Figures 6.1(b) and (c) depict two-sample t-tests on male and female subject-based saliency maps from the D_1 testing datasets (M > F and M < F) depict the brain areas that are predictive in male and female subjects.

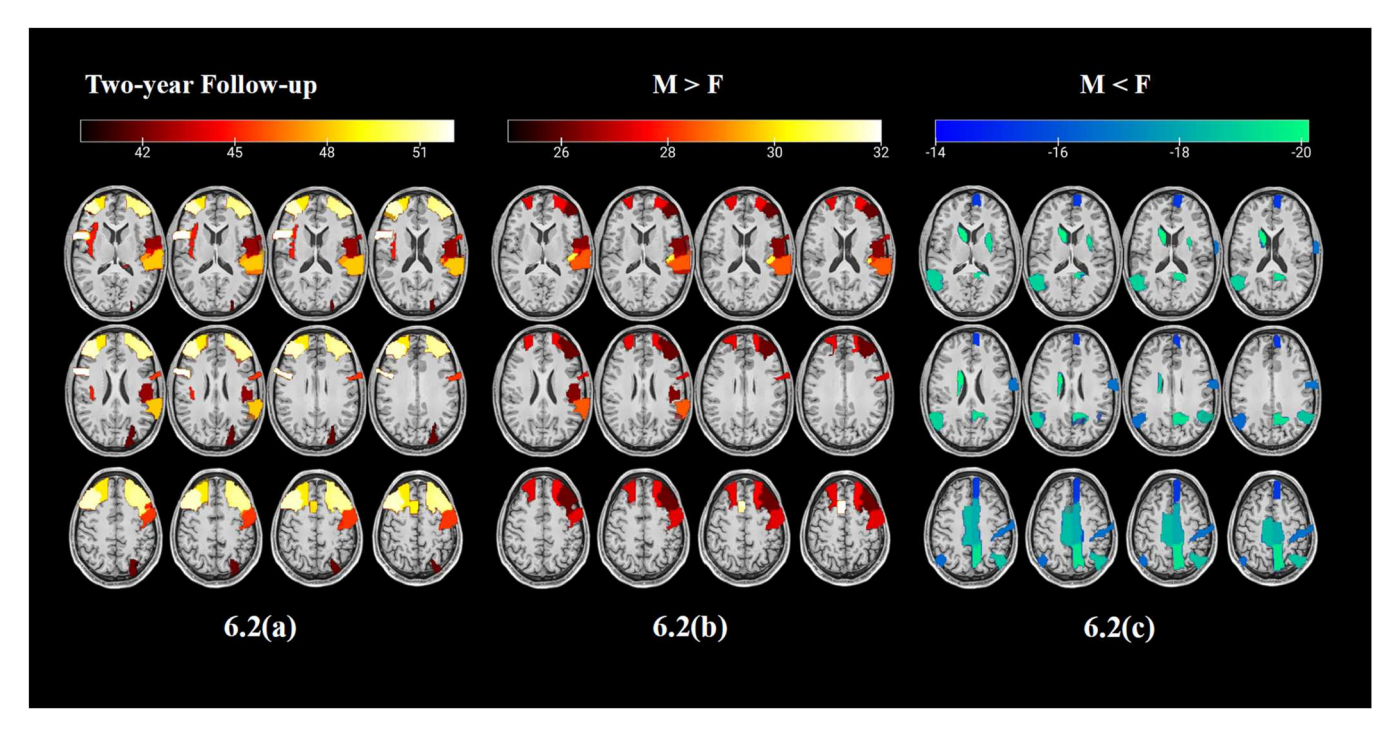


Fig. 7. (a) shows one sample t-test on subject-based saliency maps from the D_2 testing datasets; Figures 6.2(b) and (c) show two t-tests on male and female subject-based saliency maps from the D_2 testing datasets (M > F and M < F).

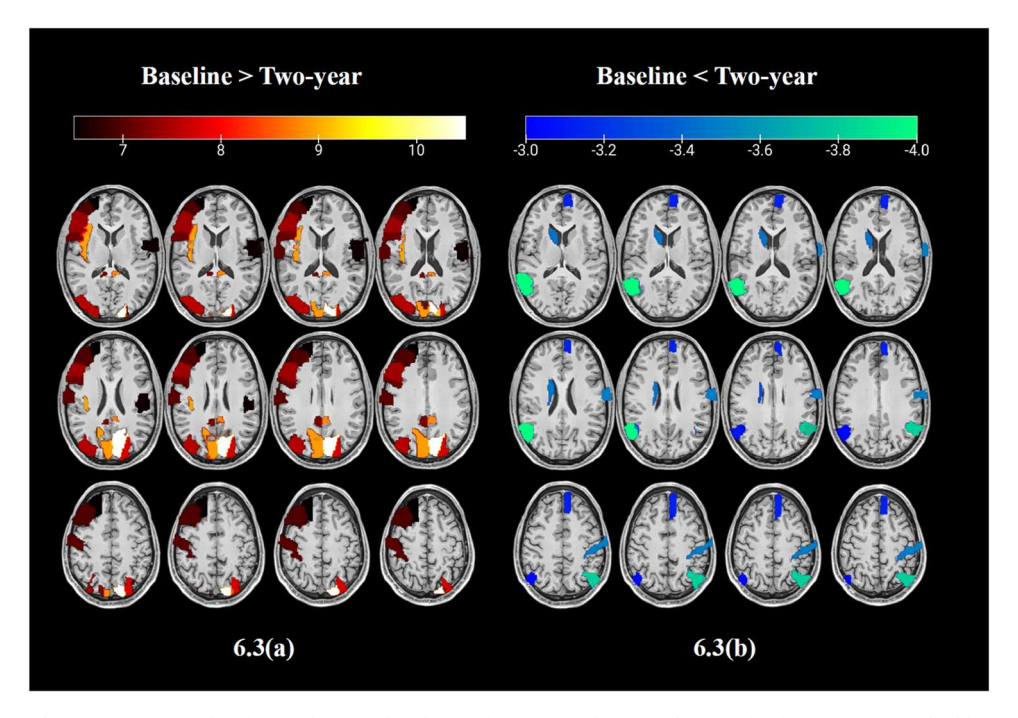


Fig. 8. (a) and (b) show saliency maps from related *t*-tests between baseline and two-year subjects, indicating that brain regions are highly predictive in baseline and two-year.

the standard SVM model to identify gender in the ABCD dataset (N=8325) and discovered both positive and negative categories between male and female brain areas.

The t-test results from baseline and two-year datasets indicate that multiple brain regions with high t-values have a statistically significant relationship with gender prediction tasks. The brain regions identified at baseline and two years of saliency maps are highlight similar. These brain regions include inferior, middle, and superior frontal gyri as well as the inferior temporal gyrus. The main difference between the baseline

and two-year saliency maps is that the middle frontal and inferior temporal gyri intensities are different. This finding indicates that important brain regions associated with gender remain relatively stable over time. We utilize the t-test to identify discrete brain areas with diverse meanings across multiple datasets and revealed that these brain regions are substantially comparable across the baseline and two-year time points. In contrast, when we analyze the different brain regions of male and female subjects with a focus on gray matter changes, we observe that the results were informative and distinctive in comparison

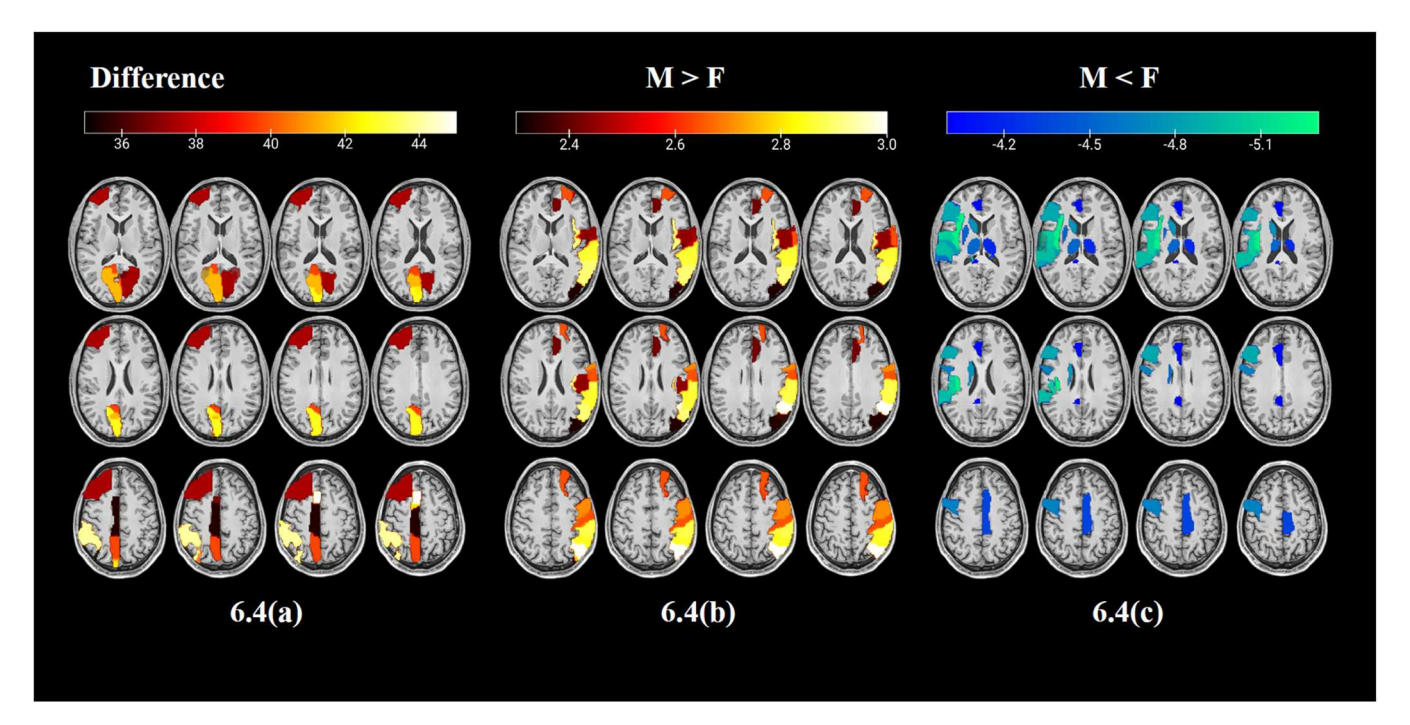


Fig. 9. (a) depicts one sample t-test using subject-based saliency maps from the D_3 datasets, which includes brain regions that are significantly relevant in voxel-wised differences between two-year and baseline data; Figure 9 (b) and (c) depict two-sample t-test using male and female subject-based saliency maps from the D_3 datasets, which can depict distinct brain regions oriented to males and females.

to baseline and two-year data. Furthermore, our research analyzes gender differences in adolescent brain structures; these brain areas are distinct between males and females and may have therapeutic applications and implications for illnesses and brain development in this age group. Choleris et al. (1873) presented several clinical research paths pertaining to gender differences that motivate us to consider potential clinical applications employing deep learning models to predict gender differences from multiple brain imaging datasets.

Additionally, we a review of studies focused on gender difference in brain structures both in adults and adolescents revealed that several research that have calculated the gender differences in adults suggest potential concordance in particular brain regions with our analysis on the adolescence dataset. For example, Zhang et al. (2020b) shows that the caudate is a distinctive part for females over males both in adults and adolescents; Ruigrok et al. (2014) shows additional brain areas that have gray matter volume differences in male and female groups, including the cerebellum in males over females, and the precuneus in females over males, consistent with our study. Other studies that concentrate on the young adult and adolescent populations also show several brain regions that are consistent with our most recent analysis of the ABCD dataset. For example, according to (Witte et al., 2010), the precuneus is a special part of the brain where females have bigger gray matter volumes than males. In contrast, the right and left cerebellum have different gray matter volumes, with females having less than males. While these studies are consistent, our is the first to highlight the salient regions in a predictive deep learning model focus solely on gray matter changes over a two-year period.

There are some limitations to our study. First, the large-scale structural MRI dataset Miller et al. (2016) is beneficial for delving further into the longitudinal study and the difference in and of itself. Since we only have 2000 more individuals for a two-year follow-up, we may not have enough data to draw firm conclusions. As additional data is released for the ABCD study, we should be able to address this in future work. Secondly, we used ROI-based saliency maps rather than voxel-wise saliency maps. We can instead leverage a voxel-wise saliency map (Taki et al., 2004), to increase spatial resolution and detail in the baseline and two-year datasets. In addition, we can use additional model

introspection approaches to highlight additional information captured by the deep learning model. The third limitation is that we did not compare different deep learning models and machine learning algorithms with ours to determine whether there was a difference in performance, including training time and FLOPs (Schulz et al., 2020). In the current study, we show our model achieved a statistically significant high accuracy on baseline gender prediction. In future work, we plan to compare it to results from other state-of-the-art deep learning models applied to similar situations.

CRediT authorship contribution statement

Yuda Bi is the first author who wrote the paper and finished all experiments in the paper; Anees Abrol, Jingyu Liu, and Jiayu Chen are responsible for comments on changing and polishing up the original article and gave suggestions; Zening Fu provided pre-processed structural MRI data which is used in experiments in the paper; Vince Calhoun is the director of our lab who is responsible for the paper ideas and also editing the article.

Data Availability

No data was used for the research described in the article.

Acknowledgements

We thank the researchers who collected the ABCD study data. Our work was supported in part by NSF grant 2112455 and NIH R01MH118695.

References

Abrol, A., Fu, Z., Salman, M., Silva, R., Du, Y., Plis, S., Calhoun, V., 2021. Deep learning encodes robust discriminative neuroimaging representations to outperform standard machine learning. Nat. Commun. 12 (1), 353. https://doi.org/10.1038/s41467-020-20655-6.

Adeli, E., Zhao, Q., Zahr, N.M., Goldstone, A., Pfefferbaum, A., Sullivan, E.V., Pohl, K.M., 2020. Deep learning identifies morphological determinants of sex differences in the

- pre-adolescent brain. Neuroimage 223, 117293. https://doi.org/10.1016/j.neuroimage.2020.117293.
- Brennan, D., Wu, T., Fan, J., 2021. Morphometrical brain markers of sex difference. Cereb. Cortex 31 (8), 3641–3649. https://doi.org/10.1093/cercor/bhab037.
- Casey, B.J., Cannonier, T., Conley, M.I., Cohen, A.O., Barch, D.M., Heitzeg, M.M., Soules, M.E., Teslovich, T., Dellarco, D.V., Garavan, H., Orr, C.A., Wager, T.D., Banich, M.T., Speer, N.K., Sutherland, M.T., Riedel, M.C., Dick, A.S., Bjork, J.M., Thomas, K.M., Dale, A.M., 2018. The adolescent brain cognitive development (ABCD) study: imaging acquisition across 21 sites. Dev. Cogn. Neurosci. 32, 43–54. https://doi.org/10.1016/j.dcn.2018.03.001.
- Chato, Land Latiff, S. (2017). Machine learning and deep learning techniques to predict overall survival of brain tumor patients using MRI images. 2017 IEEE 17th international conference on bioinformatics and bioengineering (BIBE),
- Chen, J., Wan, Z., Zhang, J., Li, W., Chen, Y., Li, Y., Duan, Y., 2021. Medical image segmentation and reconstruction of prostate tumor based on 3D AlexNet. Comput. Methods Prog. Biomed. 200, 105878 https://doi.org/10.1016/j.cmpb.2020.105878.
- Choleris, E., Galea, L.A.M., Sohrabji, F., Frick, K.M. Sex differences in the brain: Implications for behavioral and biomedical research. (1873-7528 (Electronic)).
- Gupta, C.N., Turner, J.A., Calhoun, V.D., 2019. Source-based morphometry: a decade of covarying structural brain patterns. Brain Struct. Funct. 224 (9), 3031–3044. https://doi.org/10.1007/s00429-019-01969-8.
- Hinton, G., 2018. Deep learning-a technology with the potential to transform health care. Jama 320 (11), 1101–1102. https://doi.org/10.1001/jama.2018.11100.
- Hinton, G.E. and Roweis, S. (2002). Stochastic Neighbor Embedding (https://proceedings.neurips.cc/paper/2002/file/6150ccc6069bea6b5716254057a194ef-Paper.pdf).
- Justin, S.P., Andrew, J.P., Bennett, A.L., Daniel, F. (2017). Deep learning for brain tumor classification. Proc.SPIE,
- Karcher, N.R., Barch, D.M., 2021. The ABCD study: understanding the development of risk for mental and physical health outcomes. Neuropsychopharmacology 46 (1), 131–142. https://doi.org/10.1038/s41386-020-0736-6.
- Krizhevsky, A., Sutskever, I., Hinton, G.E., 2017. ImageNet classification with deep convolutional neural networks. Commun. ACM 60 (6), 84–90. https://doi.org/ 10.1145/3065386
- Liu, M., Zhang, J., Lian, C., Shen, D., 2020. Weakly supervised deep learning for brain disease prognosis using MRI and incomplete clinical scores. IEEE Trans. Cybern. 50 (7), 3381–3392. https://doi.org/10.1109/TCYB.2019.2904186.
- Miller, K.L., Alfaro-Almagro, F., Bangerter, N.K., Thomas, D.L., Yacoub, E., Xu, J., Bartsch, A.J., Jbabdi, S., Sotiropoulos, S.N., Andersson, J.L.R., Griffanti, L., Douaud, G., Okell, T.W., Weale, P., Dragonu, I., Garratt, S., Hudson, S., Collins, R., Jenkinson, M., Smith, S.M., 2016. Multimodal population brain imaging in the UK Biobank prospective epidemiological study. Nat. Neurosci. 19 (11), 1523–1536. https://doi.org/10.1038/nn.4393.
- Osuch, E., Gao, S., Wammes, M., Théberge, J., Williamson, P., Neufeld, R.J., Du, Y., Sui, J., Calhoun, V., 2018. Complexity in mood disorder diagnosis: fMRI connectivity networks predicted medication-class of response in complex patients [https://doi.org/10.1111/acps.12945] Acta Psychiatr. Scand. 138 (5), 472–482. https://doi.org/
- Plis, S.M., Hjelm, D.R., Salakhutdinov, R., Allen, E.A., Bockholt, H.J., Long, J.D., Johnson, H.J., Paulsen, J.S., Turner, J.A., Calhoun, V.D., 2014. Deep learning for neuroimaging: a validation study. Front. Neurosci. 8 https://doi.org/10.3389/ fnips.2014.00229
- Reddy, A.V.N., Krishna, C.P., Mallick, P.K., Satapathy, S.K., Tiwari, P., Zymbler, M., Kumar, S., 2020. Analyzing MRI scans to detect glioblastoma tumor using hybrid

- deep belief networks. J. Big Data 7 (1), 35. https://doi.org/10.1186/s40537-020-00311-v.
- Ronneberger, O., Fischer, P., Brox, T. (2015, 2015//). U-Net: Convolutional Networks for Biomedical Image Segmentation. Medical Image Computing and Computer-Assisted Intervention – MICCAI 2015, Cham.
- Ruigrok, A.N.V., Salimi-Khorshidi, G., Lai, M.-C., Baron-Cohen, S., Lombardo, M.V., Tait, R.J., Suckling, J., 2014. A meta-analysis of sex differences in human brain structure. Neurosci. Biobehav. Rev. 39, 34–50. https://doi.org/10.1016/j. neubjorev.2013.12.004.
- Schulz, M.-A., Yeo, B.T.T., Vogelstein, J.T., Mourao-Miranada, J., Kather, J.N., Kording, K., Richards, B., Bzdok, D., 2020. Different scaling of linear models and deep learning in UKBiobank brain images versus machine-learning datasets. Nat. Commun. 11 (1), 4238. https://doi.org/10.1038/s41467-020-18037-z.
- Shahamat, H., Saniee Abadeh, M., 2020. Brain MRI analysis using a deep learning based evolutionary approach. Neural Netw. 126, 218–234. https://doi.org/10.1016/j. neuret 2020.03.017
- Shen, D., Wu, G., Suk, H.-I., 2017. Deep learning in medical image analysis. Annu. Rev. Biomed. Eng. 19 (1), 221–248. https://doi.org/10.1146/annurev-bioeng-071516-044442
- Sorin, V., Barash, Y., Konen, E., Klang, E., 2020. Creating artificial images for radiology applications using generative adversarial networks (GANs) – a systematic review. Acad. Radiol. 27 (8), 1175–1185. https://doi.org/10.1016/j.acra.2019.12.024.
- Taki, Y., Goto, R., Evans, A., Zijdenbos, A., Neelin, P., Lerch, J., Sato, K., Ono, S., Kinomura, S., Nakagawa, M., Sugiura, M., Watanabe, J., Kawashima, R., Fukuda, H., 2004. Voxel-based morphometry of human brain with age and cerebrovascular risk factors. Neurobiol. Aging 25 (4), 455–463. https://doi.org/10.1016/j.neurobiolaging.2003.09.002.
- Varatharajah, Y., Baradwaj, S., Kiraly, A., Ardila, D., Iyer, R., Shetty, S., & Kohlhoff, K. (2018). Predicting Brain Age Using Structural Neuroimaging and Deep Learning. bioRxiv, 497925. https://doi.org/10.1101/497925.
- Wang, X., Peng, Y., Lu, L., Lu, Z., Bagheri, M., Summers, R.M. (2017, 21–26 July 2017). ChestX-Ray8: Hospital-Scale Chest X-Ray Database and Benchmarks on Weakly-Supervised Classification and Localization of Common Thorax Diseases. 2017 IEEE Conference on Computer Vision and Pattern Recognition (CVPR).
- Witte, A.V., Savli, M., Holik, A., Kasper, S., Lanzenberger, R., 2010. Regional sex differences in grey matter volume are associated with sex hormones in the young adult human brain. NeuroImage 49 (2), 1205–1212. https://doi.org/10.1016/j. neuroImage.2009.09.046.
- Yan, W., Zhao, M., Fu, Z., Pearlson, G.D., Sui, J., Calhoun, V.D., 2021. Mapping relationships among schizophrenia, bipolar and schizoaffective disorders: a deep classification and clustering framework using fMRI time series. Schizophr. Res. https://doi.org/10.1016/j.schres.2021.02.007.
- Yan, W., Qu, G., Hu, W., Abrol, A., Cai, B., Qiao, C., Plis, S.M., Wang, Y.P., Sui, J., Calhoun, V.D., 2022. Deep learning in neuroimaging: promises and challenges. IEEE Signal Process. Mag. 39 (2), 87–98. https://doi.org/10.1109/MSP.2021.3128348.
- Zhang, L., Wang, M., Liu, M., Zhang, D., 2020. A survey on deep learning for neuroimaging-based brain disorder analysis [Review]. Front. Neurosci. 14. (https://www.frontiersin.org/article/10.3389/fnins.2020.00779).
- Zhang, X., Liang, M., Qin, W., Wan, B., Yu, C., Ming, D., 2020. Gender differences are encoded differently in the structure and function of the human brain Revealed by multimodal MRI [Original Research]. Front. Hum. Neurosci. 14. (https://www.frontiersin.org/articles/10.3389/fnhum.2020.00244).